JOURNAL OF SPACECRAFT AND ROCKETS
Vol. 41, No. 4, July–August 2004

Modeling of Chemically Reacting Flows from a Side Jet at High Altitudes

S. F. Gimelshein,* D. A. Levin,† and A. A. Alexeenko‡
Pennsylvania State University, University Park, Pennsylvania 16802

The interaction of a jet from a 60-lbf (267-N) thruster positioned on the side of a small rocket, with the rarefied atmosphere between altitudes of 80 to 160 km, is studied numerically. A multistep approach is employed, which combines the successive computation of the flow inside the thruster using a Navier–Stokes solver, the axisymmetric plume core flow, and chemically reacting three-dimensional plume-atmosphere interaction using the direct simulation Monte Carlo method, and obtains the UV radiation fields based on the flow solution. The impact of the boundary layer inside the nozzle as well as the rocket speed (5–8 km/s) and flight altitude (80–160 km) on the plume-atmosphere interaction is examined.

I. Introduction

ATMOSPHERIC interceptor (AI) vehicles currently being developed use divert and attitude reaction control systems (RCS) to perform quick maneuvers during flight. The forward and aft RCS engines provide the thrust for attitude (rotational) maneuvers (pitch, yaw, and roll) and for small velocity changes along the rocket axis (translation maneuvers). In the past few years extensive experimental and theoretical studies have been undertaken to predict RCS jet interactions with the ambient atmosphere accurately. Although significant progress has been achieved in understanding the phenomenology of the jet-atmosphere interaction, several important problems still need to be resolved, particularly with regard to supersonic and hypersonic flows at low and high altitudes.

Experimental measurements have been made to characterize the jet-atmospheric interaction in wind-tunnel facilities. However, it is difficult to scale these results[1] to flight conditions because of freestream/plume chemistry, Reynolds number, surface, and wall interference effects. Computational studies are therefore necessary to supplement and expand experimental efforts and obtain credible information on performance characteristics and flowfield structure of RCS thrusters at different altitudes. At low altitudes (up to about 60 km) the freestream-jet interaction is characterized by thin plume and bow shock waves and a jet-induced separation region in front of the divert thruster side jet.[2] The flow separation is responsible for the elevated pressure in this region and corresponding thrust amplification and might also affect the operation of optical sensors located upstream from the nozzle.[3,4] The problem of sensor contamination was considered in Ref. 5. AI vehicle aerodynamics and thruster performance at low altitudes were examined numerically by several workers, mostly using solutions of the Navier–Stokes equations.[6–9]

The jet-atmosphere interaction at high altitudes is qualitatively different from that at low altitudes. The flow separation in front of the jet becomes less pronounced and diminishes at altitudes 80 km and higher, and the effect of the atmosphere on the plume is much weaker. Because of the rarefaction, the jet interaction impact on the vehicle aerodynamics is significantly smaller. The direct simulation Monte Carlo (DSMC) method was used in Ref. 10 to compute the three-dimensional jet interaction for a corner flow configuration, and the results were compared with experimental data of surface-pressure distributions. A sharp leading-edge configuration was also used in Refs. 11 and 12 where both the kinetic (DSMC) and continuum approaches were utilized to model in detail the interaction between a continuum jet and the rarefied atmosphere. A perfect gas model was used in these studies.

A chemically reacting flow in a jet-atmosphere interaction at high altitudes was studied in Ref. 13, where a 3000-N thruster jet positioned on the side of a rocket was considered. The primary goal of the research was to analyze the possible contamination effects of the plume effluents from the side jet on an optical sensor located on the side of a cylindrically shaped small rocket. The present work is a continuation of our previous work[13] with two important changes. First, because a smaller thruster is considered the uniform nozzle exit condition used in Ref. 13 might no longer be valid. Second, because higher rocket speeds are investigated here the chemical reaction set used in the earlier work[13] has been expanded in this work.

The main goal of this work is to examine the formation of NO and OH species produced as a result of chemical reactions between atmospheric and plume species and study the impact of the nozzle boundary layer on plume backflow and surface contamination. The reason for the detailed analysis of NO and OH formation is that the ultraviolet radiation from these species has been observed in earlier space flight experiments[14] and if produced in sufficient quantity might also provide diagnostic information about the spatial dependence of the jet-atmosphere interaction.

The organization of the paper is as follows. In the following section the statement of the problem is presented along with the definition of the geometric setup and flow conditions. The numerical approach used in the computations is discussed, and the main computational steps are given for the full three-dimensional modeling of a rocket side jet interacting with the atmosphere at high flight altitudes. Then, the results of the three-dimensional DSMC modeling of a jet/atmospheric interaction are presented for uniform and nonuniform nozzle-exit parameters and for different altitudes and velocities. Finally, simulated imagery caused by the OH($A \rightarrow X$) transition of the jet/atmospheric interaction is presented.

II. Flow Conditions

A schematic of the flow geometry used to study the interaction of the atmosphere, and a RCS jet is given in Fig. 1. A small rocket is modeled as a blunted cone cylinder, and the thruster is positioned on the cylinder, immediately following the cone-cylinder junction. The Y axis coincides with the axis of the cylinder, with the tip of the vehicle nose located at $Y = 0$. The nozzle exit diameter is 7.5 cm. The flow at three flight altitudes is modeled: 80, 120, and 160 km. Table 1 gives the freestream parameters utilized for these altitudes. Three different values of the freestream velocity U_∞ were

Presented as Paper 2002-0212 at the 40th Aerospace Sciences Meeting, Reno, NV, 14 January 2002; received 21 April 2003; revision received 18 June 2003; accepted for publication 1 July 2003.

*Senior Research Associate, Department of Aerospace Engineering.
†Associate Professor, Department of Aerospace Engineering.
‡Graduate Student, Department of Aerospace Engineering.

Table 1 Freestream parameters

Parameter	Altitude, km		
	80	120	160
Temperature, K	181	354	733
Number density, molecule/m^3	4.18×10^{20}	4.73×10^{17}	3.03×10^{16}
O_2 mole fraction, %	21	9	4
N_2 mole fraction, %	79	73	57
O mole fraction, %	0	18	39

Table 2 Uniform nozzle-exit conditions

Parameter	Value
Mole fraction	H_2O (25%), CO_2 (5%), CO (23%), HCl (14%), N_2 (14%), H_2 (19%)
Velocity	2050 m/s
Temperature	979 K
Number density	3.52×10^{23} molecule/m^3
Nozzle-exit area	44 cm^2
External wall temperature	300 K

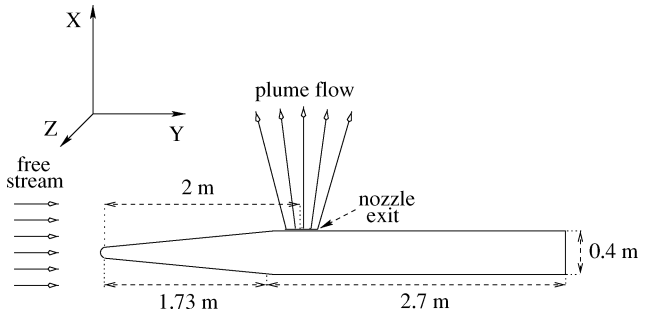

Fig. 1 Schematic of the flow.

assumed: $U_\infty = 3$, 5, and 8 km/s. A zero angle of attack is assumed in all calculations, that is, the freestream direction coincides with the rocket axis.

A 60-lbf (270-N) thruster was modeled using uniform and nonuniform distributions at the nozzle exit. The uniform exit conditions were calculated from the isentropic relations based on the chamber conditions of $P_0 = 192.5$ kPa and $T_0 = 2300$ K (see Table 2 for the complete information), whereas the nonuniform conditions were obtained from the solution of the Navier–Stokes equations inside the nozzle for the same chamber conditions. The gas compositions at the nozzle exit used in this work are those typical for small divert thrusters with a solid nonaluminum propellant.[15]

Both freestream and freestream-plume species chemical reactions were included in the simulations. The freestream chemical reaction set consists of 15 dissociation and four exchange reactions between the air species. The reaction data used for these reactions can be found elsewhere[16] (except for the data for the NO-producing first Zeldovich reaction $N_2 + O$, taken from Ref. 17). The set of chemical reactions used to model the interaction between the plume and atmospheric species and corresponding Arrhenius reaction rate constants k_r is listed in Table 3.

The set of chemical reactions has been expanded considerably from that used in earlier work.[13] Because the vehicle speeds are sufficiently high, there might be UV radiation from the NO and OH species. The NO and OH concentrations at the nozzle exit are orders of magnitude lower than the major plume species so that radiation from upper electronic states of these molecules will originate from collisional excitation of the chemically formed NO and OH species in their ground states. The first four chemical reactions between freestream species (N_2, O_2, O) and the water in the plume represent possible decomposition and exchange reactions that result in the production of OH. The hydroxyl radical can also be produced by exchange reactions of $O_2 + H$ and $H_2 + O$, with the latter reaction potentially a significant source because H_2 is a major plume species.

Table 3 Freestream-plume species reactions

Reagent	Product	A	B	E_r[a]
$N_2 + H_2O$	N_2+OH + H	5.81×10^{-15}	0.0	7.314×10^{-19}
$O_2 + H_2O$	$O_2 + OH + H$	1.13×10^{-7}	−1.31	8.197×10^{-19}
$O + H_2O$	$O + OH + H$	1.13×10^{-7}	−1.31	8.197×10^{-19}
$O + H_2O$	2OH	3.8×10^{-21}	1.3	1.275×10^{-19}
H + O_2	OH + O	1.66×10^{-16}	0.00	1.061×10^{-19}
$H_2 + O$	OH + H	3.12×10^{-16}	0.00	9.518×10^{-20}
O + HCl	OH + Cl	5.6×10^{-27}	2.87 =	2×10^{-20}
OH + Cl	O + HCl	3.1×10^{-27}	2.91	7×10^{-21}
$N_2 + O$	NO + N	9.45×10^{-18}	0.42	5.925×10^{-19}
CO + O	O + C + O	6.69×10^{-15}	0.0	1.35×10^{-18}
$CO + O_2$	$O_2 + C + O$	1.46	−3.52	1.776×10^{-18}
$CO + N_2$	$N_2 + C + O$	1.46	−3.52	1.776×10^{-18}
$N_2 + CO_2$	$N_2 + CO + O$	8.85×10^{-19}	0.5	6.072×10^{-19}
$O_2 + CO$	$O + CO_2$	4.2×10^{-18}	0.0	3.312×10^{-19}
$O + CO_2$	$O_2 + CO$	2.8×10^{-17}	0.0	3.657×10^{-19}

[a] $k_r = AT^B \exp(-E_r/kT)$, k_r is in m^3/s, and E_r is in J.

The two chemical reactions involving chlorinated species are included because HCl is a major chemical species in the plume. It is expected that these reactions will be significant and can further serve as a source for the formation of OH. These reactions also represent mechanisms for the formation of free chlorine radicals, an important precursor in atmospheric models of ozone depletion. The exchange reaction between $N_2 + O$ to produce NO is the first Zeldovich reaction, as is used in the freestream air chemical reactions. In this case, however, the sources of the molecular nitrogen and atomic oxygen species are from the plume and freestream, respectively.

The remainder of the reactions represents formation and destruction mechanisms of CO, another major plume species. The N_2, O_2, and O species are freestream species, and CO and CO_2 represent plume species with CO about a factor of five greater in concentration than carbon dioxide. CO and CO_2 are not expected to produce significant radiation in the UV through visible spectral radiation regions. The main mechanism for observing continua visible radiation from carbon dioxide involves a three-body interaction, which is not likely in the flows being considered here. It is possible that CO can radiate in the vacuum ultraviolet in the CO Cameron bands; however, this transition is forbidden and also not considered here further. Radiation from CO and CO_2 is important in the midwave infrared spectral region; however, the detailed modeling of such radiation is complex and will be considered in future work.

III. Numerical Technique

The problem under consideration is characterized and complicated by the flow three dimensionality, chemical reactions, and the large variation in number density between the thruster exhaust plume and the ambient atmosphere. The three-dimensional nature of the flow and the need to simulate a large set of chemical reactions contribute to the computational complexity of the problem. In addition, the large density variation poses difficulties with respect to the choice of an applicable numerical method. The choice of the governing equations, and thus the modeling approach for a flow problem, is based on the flow regime. The flow regime in the jet/atmospheric interaction region changes from continuum inside the nozzle (the mean free path of the order of 10^{-7} m) through transitional in the near field to almost free molecular in the far field at high altitudes (the mean free path of the order of 100 m at 160 km). That means a continuum approach needs to be applied to model the flow inside the nozzle, whereas a kinetic approach has to be used to simulate the external plume flow and the interaction of the plume with the ambient atmosphere.

The most widely used and powerful kinetic technique is the DSMC method,[18] a method that has been shown to be efficient for various gas dynamic problems in the free-molecular, transitional, and near-continuum flow regimes. The DSMC method becomes prohibitively expensive when it is applied to modeling three-dimensional flows at very low Knudsen numbers. Because the gas density for the flow of interest is very high at the thruster exit, a full three-dimensional modeling of the jet-atmosphere interaction

problem would require a prohibitively large number of simulated molecules to be used.

An effective way of simulating the jet flow is to make use of the fact that the jet coreflow is axisymmetric because it is too dense to be affected by the rarefied freestream. One therefore can split the plume flow into two regions: the plume near field where the flow is essentially axisymmetric and the region of the three-dimensional freestream-plume interaction. The latter also includes the region of the freestream-rocket body interaction. The general idea is to obtain an axisymmetric solution for the first region, use the solution to generate a starting surface expanding a few meters away from the nozzle exit, and perform successive three-dimensional simulations utilizing the generated starting surface. The density at the starting surface has to be sufficiently low for the three-dimensional DSMC modeling to be feasible, but at the same time high enough for the core flow not to be significantly affected by the free stream. The four-step numerical procedure used is therefore as follows.

Step 1

The continuum method is applied to calculate the flow inside the nozzle and in the vicinity of the nozzle exit. The solution of the Navier–Stokes equations with a finite volume spatial discretization on a structured grid is obtained with the General Aerodynamic Simulation Program (GASP).[19]

The code uses a finite volume spatial discretization on structured three-dimensional grids. Three-zone grids resolving gradients near the wall boundaries and along the axis have been used. The computational domain included the converging and diverging nozzle sections and an external plume region (Fig. 2). The total number of cells was 18,000. Viscous derivative terms in the momentum and energy conservation equations are computed with the second-order accuracy on the interior and gas–solid interface cells. A third-order upwind-biased scheme is applied for spatial reconstruction of volume properties on cell boundaries. To obtain the steady-state solution, a two-factor approximate factorization is used for time stepping. A no-slip boundary condition is used in these computations at the gas-surface interface with an internal fixed wall temperature of 1000 K. The inlet conditions are obtained from one-dimensional ideal nozzle theory based on stagnation gas properties and the inlet area ratio. A first-order extrapolation condition is applied at the outer boundary of the computational domain.

Step 2

An axisymmetric modeling of the plume corefow with the DSMC method is the second step. An axisymmetric capability of a multitask DSMC-based computational tool, SMILE,[20] is utilized in this work. The plume is modeled as a six-species (see preceding section) nonreacting gas mixture expanding into a vacuum. The plume temperatures are on the order of 1000 K; therefore, chemical reactions inside the core of the plume are not important. The inflow boundary is the nozzle exit with the parameters taken from the Navier–Stokes solution obtained at step 1.

The following DSMC models are used in the axisymmetric computations. The variable hard sphere (VHS) model[21] is used for molecular collisions, with molecular diameters taken from Ref. 18, and a value of the exponent in the viscosity-temperature dependence of 0.25. The continuous Larsen–Borgnakke model[22] with temperature-dependent rotational and vibrational relaxation numbers is used for the energy exchange between translational and internal molecular modes. The number of molecules used in the computations is about 6 million, and the number of collision cells is about 1.6 million.

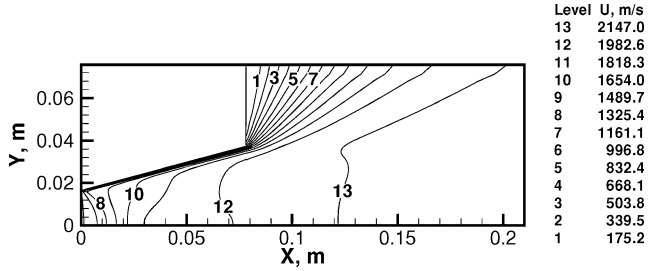

Fig. 2 *X*-velocity component contours obtained from the Navier–Stokes solution. The origin of the coordinate system is located at the nozzle throat center.

Step 3

The most challenging step of the calculation is the modeling of the jet-atmosphere interaction. The three-dimensional SMILE tool is used to compute the interaction of the freestream and plume species. The gas is considered a 15-species reacting mixture. A starting surface obtained with the axisymmetric DSMC code is used to simulate the plume inflow.

The VHS and the Larsen–Borgnakke models were used in the computations. The total collision energy (TCE)[21] model was applied to model gas-phase chemical reactions. A weighting scheme[23] applicable for chemical reactions was used to enhance the statistical representation of free stream species. The diffuse model with full energy and momentum accommodation was taken for the gas-surface interaction, with the rocket (external) wall temperature of 300 K. The total number of cells is about 8 million (from 6 to 10 million depending on the freestream and plume parameters), and the number of simulated molecules was in the range of 15 to 20 million. These numerical parameters were chosen to eliminate the grid dependence of the results and reduce the influence of statistical dependence between the simulated particles (see Ref. 13 for more details).

Step 4

The density and temperature flowfields obtained at step 3 are used to calculate UV radiation produced by NO and OH species. The NEQAIR[24] code modified as described next is used for this purpose.

The steady-state solution of the three-dimensional DSMC flow provides a grid of macroscopic parameters such as species temperatures and concentrations necessary to calculate radiation from the flow. In this work only chemical processes involving ground-state species have been considered. Excited states produced directly through chemiluminescent reactions can be important in rarefied flows for the 8-km/s case and will be considered in future work. The relevant macroscopic parameters from the three-dimensional DSMC flow solutions are used as input to the NEQAIR radiation model, a tool used extensively in the aerothermochemical community.[25] Integrated radiation from 270 to 340 nm for the OH($A \rightarrow X$) band transition and from 190 to 440 nm for the NO gamma-, beta-, and delta-band system transitions have been considered, separately.

The radiation model consists of two major components: excitation and line-by-line radiative transport. The collisional portion of the NEQAIR model[25] uses a master set of finite-rate equations to model the population of the atomic and molecular electronic state levels. The distribution of vibrational and rotational states in each electronic level is assumed to be described by a Boltzmann distribution at the gas vibrational and rotational temperatures. Previous work[26] has shown that for nonionized flows (negligible electron concentrations) the bulk flow translational temperature is the governing temperature for establishing a quasi-steady state of electronic levels. For the flow conditions modeled here, the degree of rarefaction is much higher, and the translational temperatures of the radiating species, NO and OH, are significantly different from the bulk. Therefore, for these calculations it is assumed that the governing temperatures for establishing the steady-state distributions of electronic states are the OH- and NO-species translational temperatures. The steady-state distributions are used to calculate emission at each point in the flow, which is then integrated along a line of sight using the accurate NEQAIR line-by-line radiative transport model. The spectral database for the OH and NO ultraviolet emissions is extensive and documented elsewhere.[24,25]

IV. Flow Inside the Nozzle

First, the flow inside an RCS nozzle has been calculated by the continuum method using the parameters and models discussed in

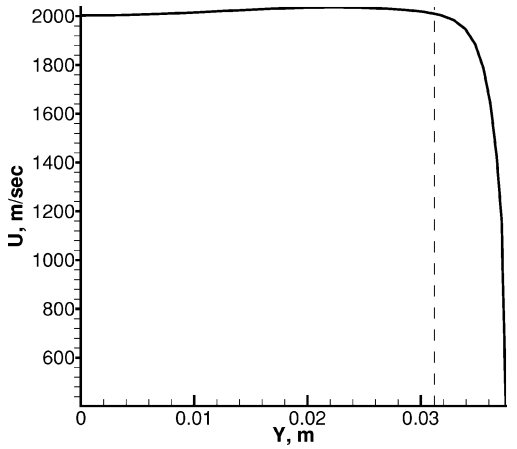

Fig. 3 Continuum results for the axial component of velocity along the nozzle exit. Nozzle axis is at $Y = 0$; wall is at $Y = 0.0375$ m.

the preceding section. Uniform parameters were taken at the nozzle inlet, calculated from the chamber condition using isentropic relations. The flow was simulated as a one-species gas with a constant specific heat ratio of 1.3 and molecular mass of 3.675×10^{-26} kg. Such a gas approximates reasonably well the six-species gas mixture given in Table 2.

The flow structure in the diverging part of the RCS nozzle is shown in Fig. 2, where the X component of velocity is plotted. The Navier–Stokes solution predicts that the gas expansion in the nozzle is influenced by two-dimensional and viscous effects, and, thus, nozzle-exit parameters differ from those obtained using one-dimensional ideal nozzle theory (Table 2). Figure 3 shows the axial component of velocity at the nozzle exit. The thickness of the boundary layer, the distance from the wall at which the value of velocity is 99% of that at the axis, is 16% of the exit radius. The boundary-layer region is from the dashed line to the wall ($Y = 0.0375$ m), as shown in Fig. 3.

V. Modeling of the Axisymmetric Plume Core

The density, velocity, and temperature profiles at the nozzle exit (obtained from the calculations discussed in Sec. IV) were extracted and then used as inflow boundary conditions for the successive axisymmetric DSMC calculations of the plume core. The axisymmetric DSMC code was used to calculate the plume core not affected by the rarefied freestream. The inflow boundary condition was set at the nozzle exit, and the vacuum boundary condition was used at the downstream boundaries. Two inflow conditions were used: uniform and nonuniform (Navier–Stokes). The sensitivity of the near-field flow along the nozzle axis to the uniform vs nonuniform conditions is small. However, the variation of number density at a cross section located at 0.5 m from the exit (Fig. 4) for uniform and nonuniform exit conditions provides a quantitative measure of the influence of the boundary layer on the near-field plume. The density for the nonuniform profile is more than an order of magnitude larger at the plume periphery (i.e., angles larger than 60 deg from the nozzle axis). This difference will be shown to affect the jet-atmosphere interaction and surface contamination.

VI. Three-Dimensional Jet/Atmosphere Interaction

A. Sensitivity to the Exit Conditions

First, we discuss the computational results that illustrate the effects of constant and nonuniform nozzle-exit conditions on the jet/atmosphere interaction. The results are presented for an altitude of 120 km and a freestream velocity of 5 km/s. Figure 5 shows the comparison of the nitrogen number density fields for the two nozzle-exit conditions. Generally, the difference between the two fields is caused by a larger plume expansion for the nonuniform case (see Fig. 4). The boundary layer near the nozzle lip causes more particles to move off the axis compared to the uniform case. This, in turn, results in a larger distance between the shock created by the freestream interacting with the plume (plume shock hereafter) and

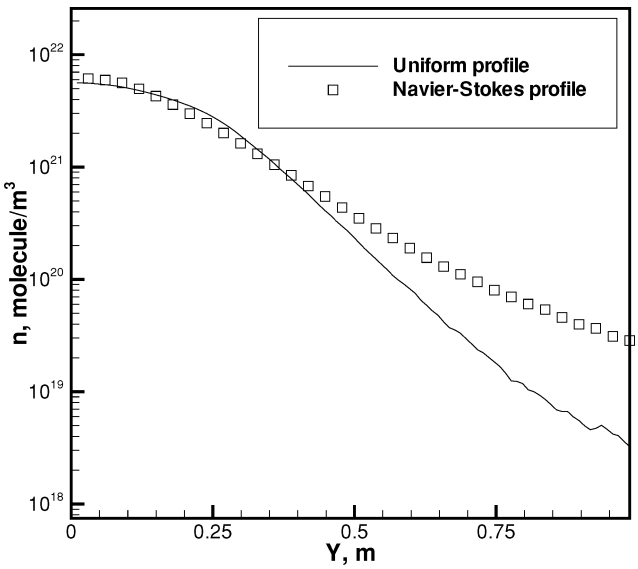

Fig. 4 Number density profiles (molecule/m^3) for different inflow conditions in the cross section perpendicular to the nozzle axis at 0.5 m downstream from the exit.

the nozzle axis. For the uniform conditions there is a local maximum in the number density that occurs in the middle of the conical part of the body (see the insert in Fig. 5) that is not observed for the nonuniform conditions. In addition, Fig. 5 shows a stronger N_2 density gradient across the shock for the nonuniform conditions because of the larger spread of the plume and greater relative velocities between the freestream and plume molecules.

The distributions of the total mass fluxes on the surface are shown in Fig. 6 for the constant and nonuniform nozzle-exit conditions. For the nonuniform case there is a noticeable maximum on the cylindrical part that is formed by the plume backflow. In contrast, this effect is not observed for the uniform exit conditions. There is also a local maximum on the cone tip that is formed as a result of the plume-jet interaction for the nonuniform conditions. Such a maximum is also observed for the uniform exit conditions, but it is shifted downstream as a result of the smaller spread of the plume. The simulation results also show that the mass flux on the forebody is mostly caused by the freestream species, whereas on the cylindrical part it originates principally from the lightest species of the plume, molecular hydrogen.

Finally, let us consider the impact of the nozzle boundary layer on the formation of the NO and OH species. The nitric-oxide species is formed by reactions of freestream atomic oxygen with plume N_2. In contrast, the hydroxyl radical can be formed by one or several of the first seven reactions given in Table 3. Reactions of plume species H_2O and HCl with freestream atomic oxygen were found to be the most important processes. Generally, the effect of nonuniform exit conditions is to increase the NO and OH density gradients across the shock and to produce higher concentrations of NO and OH caused by the greater relative velocities of the colliders. The quantitative impact of the nozzle-exit conditions on NO production can be been seen in Fig. 7, where the NO number density as a function of position along an axis parallel to the rocket axis at a height of 3 m from the nozzle exit is shown. Comparison of the two NO number density profiles for uniform and nonuniform conditions shows that the location of the maximum for the latter case is shifted upstream, farther from the jet, compared to the uniform nozzle exit case. The maximum of the number density is two times larger for the nonuniform conditions. The nozzle-exit conditions also affect the degree of OH production, although the impact is somewhat smaller than for NO formation. Figure 7 shows that the OH number density maximum is about 20% higher for the nonuniform condition.

The results discussed in this subsection show that the nozzle boundary layer has an important effect on the freestream-plume chemistry. Hereafter, we will only consider the nonuniform nozzle-exit condition.

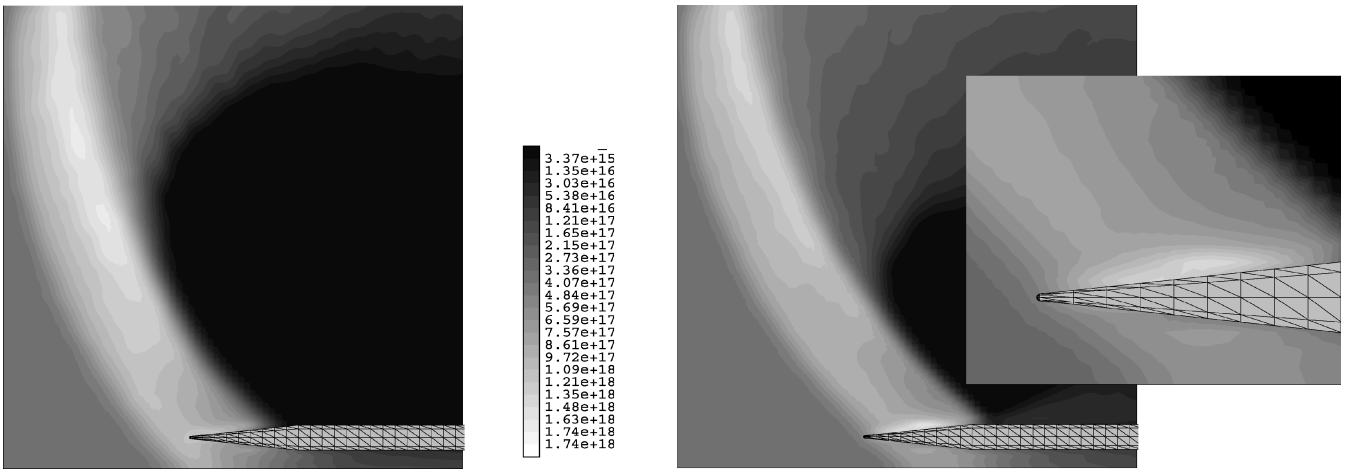

Fig. 5 Freestream N_2 number density contours (molecule/m^3) for nonuniform (left) and uniform (right) exit conditions for an altitude of 120 km and a freestream velocity 5 km/s. The *XY* plane is shown with an area of 7.4×7.5 m.

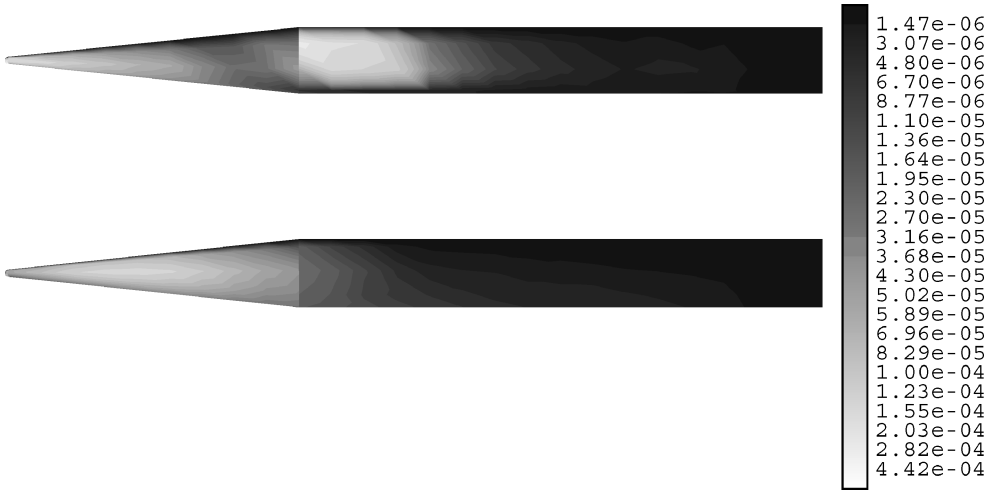

Fig. 6 Distribution of the total mass flux (kg/m^2-s) on the vehicle upper surface (containing the thruster) for nonuniform (top) and uniform (bottom) exit conditions and an altitude of 120 km and a freestream velocity of 5 km/s.

B. Sensitivity of the Flow Solution to Altitude

We next consider the effect of freestream number density and freestream species concentrations on the jet/atmosphere interaction. Figures 8 and 9 show the variation in Mach-number and OH number density contours for altitudes of 80, 120, and 160 km. The figures show that as altitude is increased the jet/atmosphere interaction becomes more diffuse. In Fig. 8 for 80 km the flowfield exhibits continuumlike features such as an oblique shock wave and a normal plume shock, which induces flow separation. At a higher altitude of 120 km, the shock structure is much more diffuse than at 80 km. The extent of the plume expansion is much greater than at 80 km, and a nearly normal plume/atmosphere interaction shock is still formed. Finally, at 160 km the plume/atmosphere interaction shock is replaced by a much diffuser interaction zone. Figure 9 reflects changes in the flow structure observed for the OH number density number contours at different altitudes similar to those observed in the Mach number contour fields. Because the hydroxyl radical is formed by collisions of plume and freestream species, it will mainly exist in the plume/atmosphere interaction region. Note, in Fig. 9 the change in magnitude of the peak OH concentration at the three altitudes is approximately proportional to the changes in freestream number density.

C. Impact of the Vehicle Velocity

The vehicle velocity also has an important effect on the flowfield structure. Figures 10 and 11 show the variation in translational temperature and OH number density contours for freestream velocities of 3, 5, and 8 km/s at an altitude of 120 km. As the freestream velocity increases, the temperature inside the plume shock also increases, and the location of the shock moves closer to the body. As expected, the large rise in temperatures (compare the maximum of about 9000 K for 3 km/s and 36,000 K for 8 km/s) results in much higher reaction rates for the 8-km/s case, as is clearly seen in Fig. 11. The maximum of the OH density occurs further downstream for higher velocities, and the value of this maximum is almost two orders of magnitude larger for 8 km/s than for 3 km/s. Note that similar trends were observed for the NO production, with the difference being even more pronounced than for OH because of the greater reaction threshold.

As was just mentioned, the first eight reactions in Table 3 potentially contribute to the steady-state OH radical concentration. The first three reactions represent OH formation by collisionally induced dissociation of water by freestream species, N_2, O_2, and O. Reactions 4 and 6 represent the formation of OH by exchange reactions of freestream atomic oxygen with either water or molecular hydrogen in the plume. Finally, the hydroxyl radical can be formed by freestream O exchange reactions with plume HCl. Analyzing which of the reactions are important for different combinations of freestream altitudies and velocities is complicated by the different reaction thresholds E_r and change in freestream species concentrations. Analyses of the flowfields presented in this work indicate that the three most important reactions for OH production are water exchange with atomic oxygen, water dissociation by nitrogen, and hydrochloric acid exchange with atomic oxygen. Although there is approximately 20% molecular hydrogen at the plume nozzle exit,

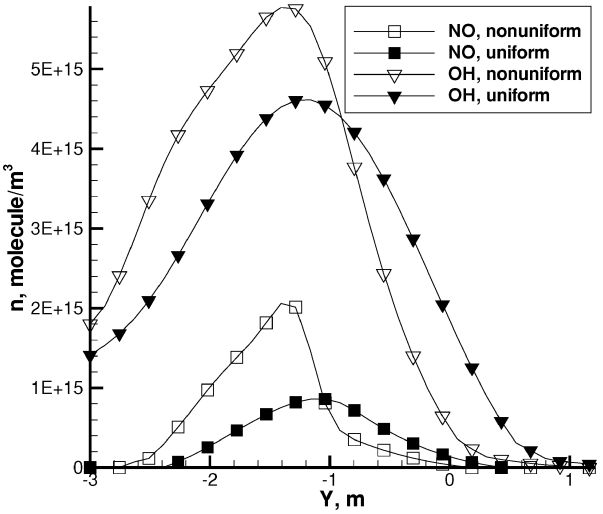

Fig. 7 NO and OH number density profile (molecule/m^3) for different exit conditions at $X = 3$ m from the vehicle axis in the XY symmetry plane at an altitude of 120 km and a freestream velocity of 5 km/s.

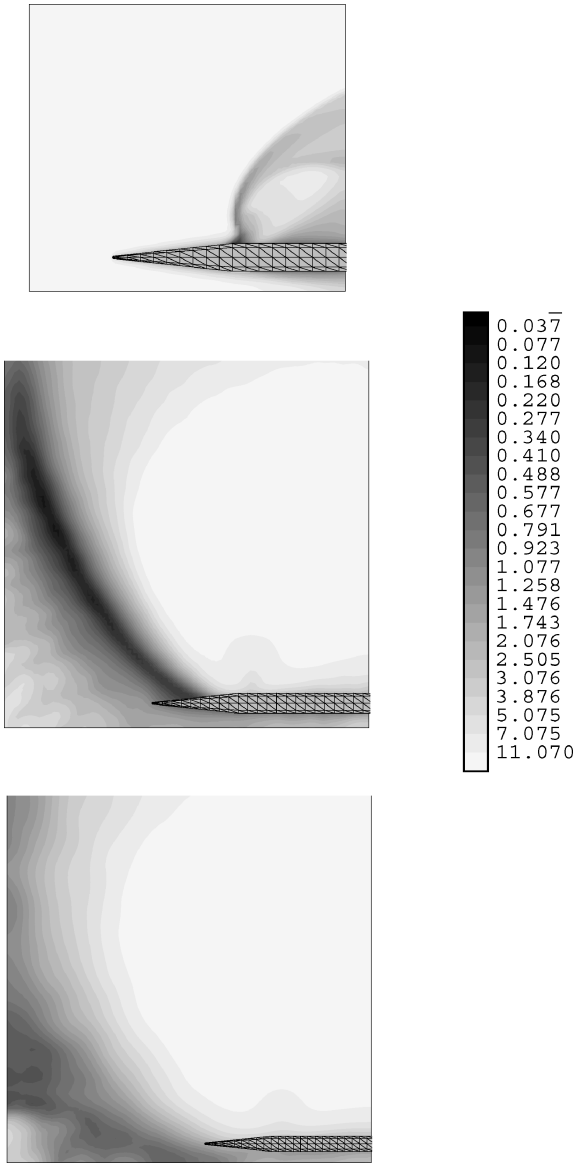

Fig. 8 Mach-number contours at different altitudes: top, 80 km, area shown is 4.66×4.2 m; middle, 120 km, area shown is 7.4×7.5 m; and bottom, 160 km, area shown 9×9.8 m. The vehicle velocity is 5 km/s in all of the cases.

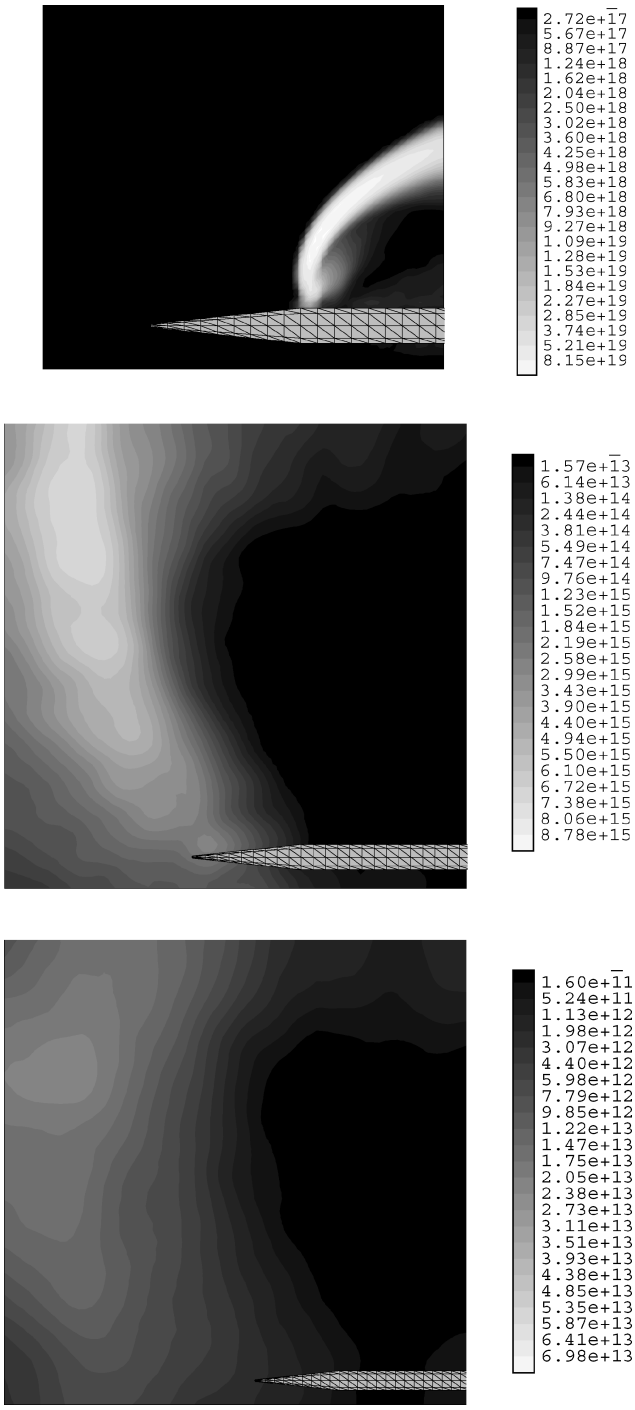

Fig. 9 OH number density (molecule/m^3) contours at different altitudes: top, 80 km, area shown is 4.66×4.2 m; middle, 120 km, area shown is 6.6×7.5 m; and bottom, 160 km, area shown is 9×9.8 m. The vehicle velocity is 5 km/s in all of the cases.

the threshold for the reaction of molecular hydrogen with atomic oxygen is too high for the flow conditions discussed here. The low reduced mass of the O-H_2 pair (compared to other flow reactants) leads to a translational energy below the reaction threshold. For freestream velocities of 5 km/s and higher and an altitude of 80 km, the OH formation by water exchange with atomic O was found to dominate and contributed more than 50% of the OH produced. However, for the same speeds, but altitudes of 120 km and higher, oxygen exchange with HCl was found to contribute more than 70% of the OH produced. Because there is no freestream atomic oxygen at 80 km, the rate of dissociation of freestream molecular oxygen is low, and the reaction threshold is lower for the O + HCl reaction; it is not clear why water exchange with O should dominate. Moreover,

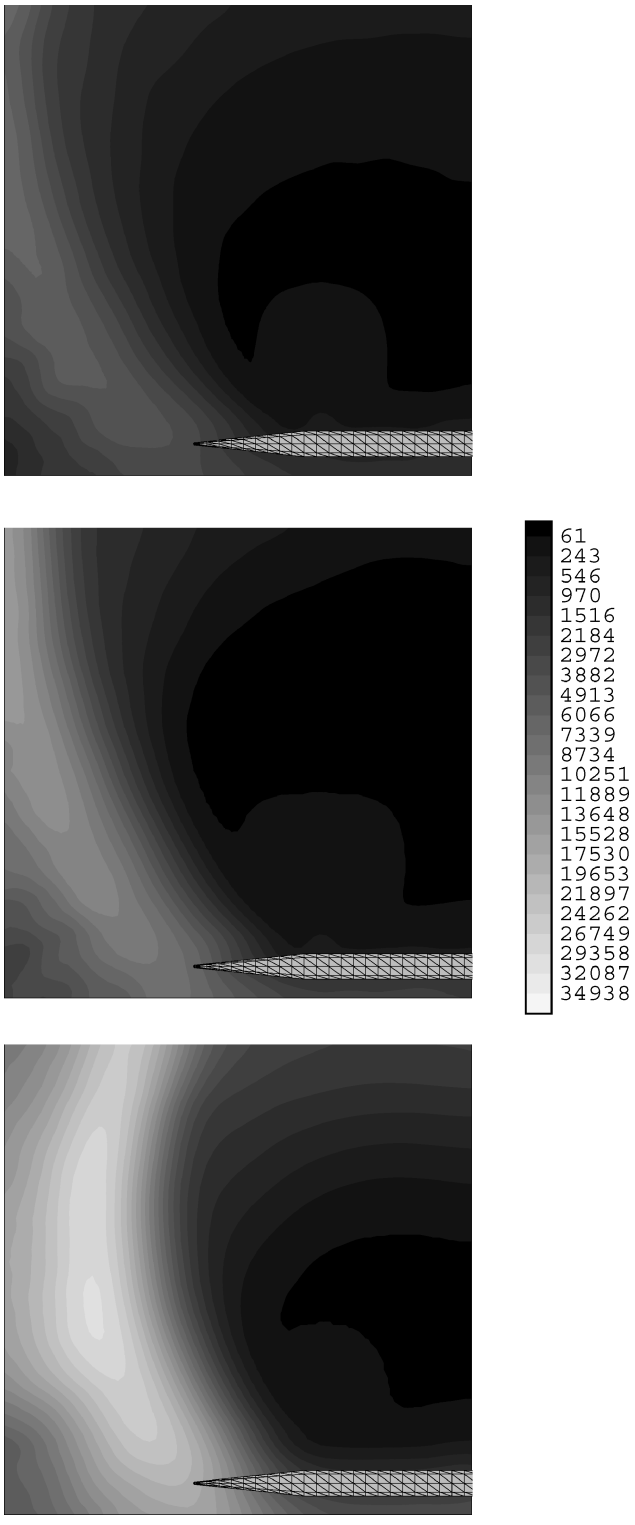

Fig. 10 Translational temperature (K) contours at the altitude 120 km for different freestream velocities: top, 3 km/s; middle, 5 km/s; and bottom, 8 km/s. Area shown is 6.3×7.5 m.

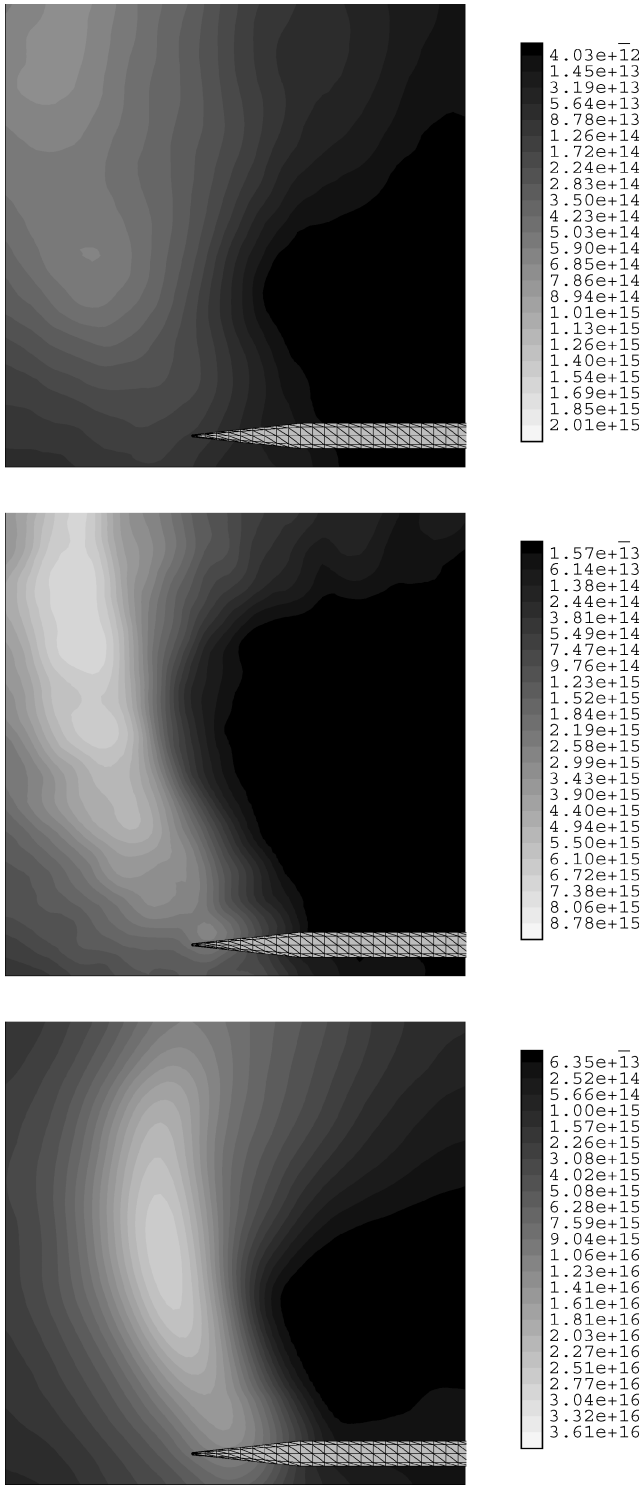

Fig. 11 OH number density (molecule/m^3) contours at the altitude 120 km for different freestream velocities: top, 3 km/s; middle, 5 km/s; and bottom, 8 km/s. Area shown is 6.5×7.5 m.

the dramatic reversal in the relative importance of the two reactions for the higher altitudes is inconsistent as well.

To understand this apparent discrepancy, we must consider the reaction rate for O + HCl used[27] in this work. The experimental rate coefficient was found for temperatures between 350 and 1490 K, which are much lower than the temperatures observed in the plume-shock interaction. The more recent work of Hsiao et al.[28] extended the rate measurements up to temperatures of 3200 K, which were found to be consistent with the earlier work.[27] However, the high temperature exponent for both sets of measurements (2.87 in Table 3 and 3.67 in Ref. 28) indicate that the rate coefficient significantly increases at high temperatures as the preexponential term in the Arrhenius equation becomes dominant. The total collision cross section, determined by the VHS model in this work, weakly depends on temperature. All of these factors lead a case where the reaction rate for the O + HCl reaction is larger than the collision rate at temperatures larger than 6000–7000 K. As a result, the reaction probability becomes larger than one for the TCE chemistry model[29] used here. Note that this could be a problem for any other chemistry

reaction model that is based on the use of the Arrhenius form for the experimental rate. The specific implementation used here was to model a single reaction in all cases, if the reaction probability were larger than one. This essentially causes a much smaller number of reactions to occur in the simulation compared to that governed by the Arrhenius equation. The situation is even more complicated by the fact that flow is in thermal nonequilibrium, which means that the chemical rate might be different from the experimanal one obtained under conditions close to equilibrium.

As a result, the present assessment of the proportions of the three chemical reactions is probably poor. To remedy this situation, however, fundamental chemical physics reaction modeling and experiments of hypervelocity collision cross sections are required. Finally, examination of the chemical physics literature shows that the $HCl + O$ rate modeling and experimental data is at sufficiently low temperatures that one can neglect the second reaction channel ($HCl + O \rightarrow ClO + H$). This channel, however, is accessible for the collisions considered here and would reduce the reaction probability if the branching ratios were known.

VII. UV Radiation

The radiation can now be calculated using the temperature and concentration fields just discussed. An onboard imager array would measure integrated radiance values summed along a matrix of lines of sight for each pixel element of the array. The resultant simulated images would therefore depend on the specific placement of the imager relative to the side-jet thruster.

To develop a general idea about the possible image features, the three simplest viewing geometries were considered for OH radiation at the freestream conditions of 8 km/s for 80 and 120 km. Figures 12–14 show the integrated radiances for viewing along the z, x, and y axes of Fig. 1, respectively. Comparison of Figs. 12 and 13 shows that the shape of the integrated radiation from the OH plume shock is essentially the same in the y and z directions with similar absolute magnitudes. Comparisons of calculations performed with and without full radiative transport demonstrate that the OH UV radiation are optically thin. Integration for lines of sight in front of the plume shock (Fig. 14) results in about a factor of four reduction in integrated radiance caused by an effectively smaller radiating length in that direction. Finally in Fig. 15 we present normalized radiance contours integrated normal to the rocket velocity (z direction) for the freestream condition of 80 km at 5 km/s. The spatial distribution of the integrated OH radiance is similar to the OH distribution in the shock shown earlier in Fig. 9.

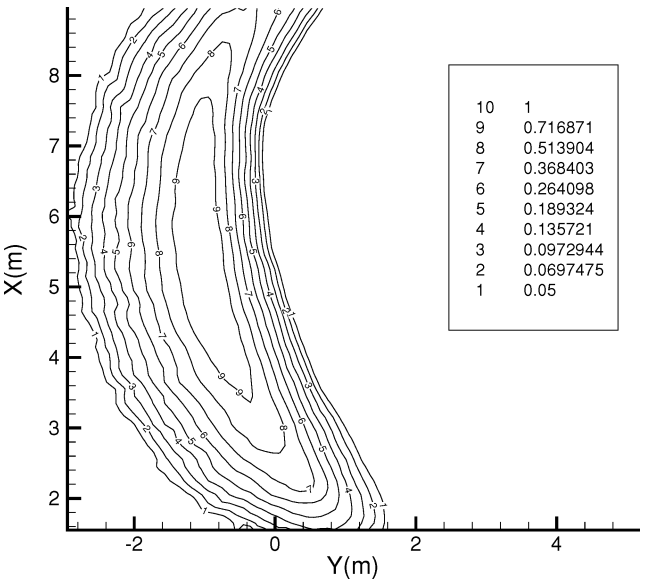

Fig. 12 Integrated OH UV radiation (W/cm^2-sr) along the z axis at 8 km/s for an altitude of 120 km. The contour values are normalized to the maximum value of 1.52×10^{-2}.

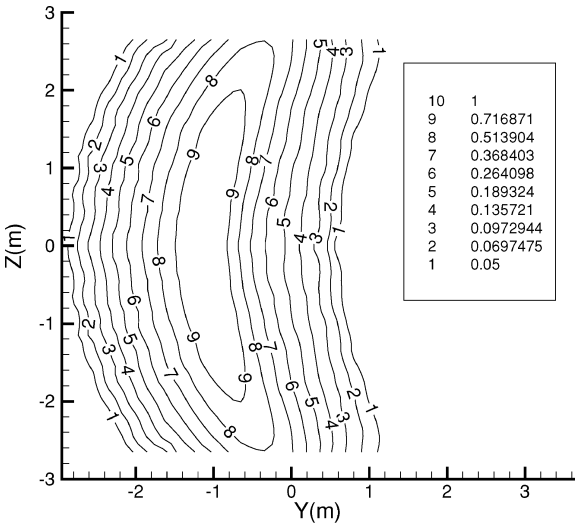

Fig. 13 Integrated OH UV radiation (W/cm^2-sr) along the x axis at 8 km/s for an altitude of 120 km. The contour values are normalized to the maximum value of 1.69×10^{-2}.

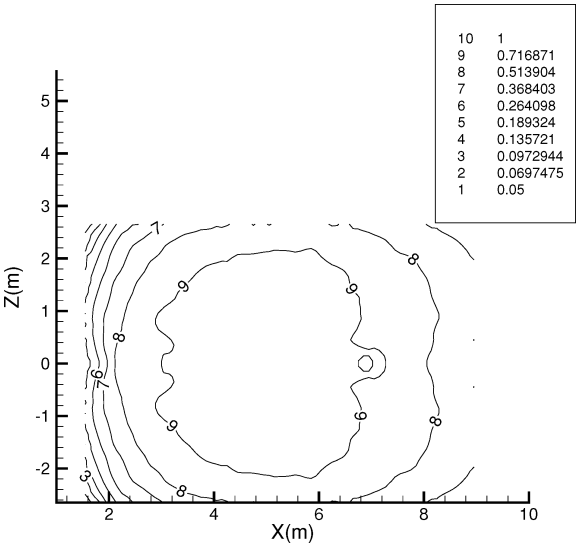

Fig. 14 Integrated OH UV radiation (W/cm^2-sr) along the y axis at 8 km/s for an altitude of 120 km. The contour values are normalized to the maximum value of 4.42×10^{-3}.

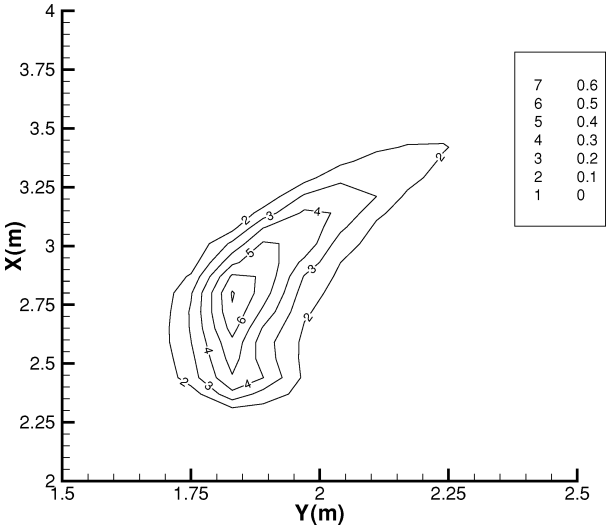

Fig. 15 Integrated OH UV radiation (W/cm^2-sr) along the z axis at 5 km/s for an altitude of 80 km. The contour values are normalized to the maximum value of 0.44.

Radiation fields were studied for the NO UV radiation as well. The radiation was found to be optically thin with slighty narrower spatial distributions than that obtained for OH radiation. The main difference between the NO and OH radiation fields and simulated images is the maximum radiance value. For freestream velocities of 5 and 8 km/s, the NO values are typically about two to three orders of magnitude weaker than OH. Unlike OH, there is no detectable NO radiation at a freestream velocity of 3 km/s. The magnitude of the NO radiation is more sensitive to the freestream velocity than OH caused by the higher reaction and radiation threshold.

VIII. Conclusions

The interaction of a jet from a side-mounted 60-lbf thruster with the rarefied atmosphere between altitudes of 80 and 160 km has been modeled. The direct simulation Monte Carlo method was applied to model the three-dimensional jet-atmosphere interaction. Chemical reactions between freestream and plume species were included in the external jet simulations. Both uniform and nonuniform conditions were used at the thruster exit. A Navier–Stokes solver is used to calculate flow inside the thruster and in the near field of the plume. A two-stage numerical strategy was then used to calculate the plume, with sequential computations of an axisymmetric plume core flow, and three-dimensional plume-freestream interactions. The impact of rocket velocity and altitude on the plume-atmospheric interaction in terms of species produced by chemical reactions that can contribute to UV radiation was examined.

The internal nozzle flow simulation demonstrated that the boundary layer subsumes approximately 16% of the nozzle-exit radius. Navier–Stokes and DSMC computations were found to be in good agreement in the vicinity of the nozzle exit. The differences in the uniform and nonuniform nozzle-exit profiles were found to affect the plume and freestream species, as well as those species produced by chemical reactions. Plume species were found to exist further upstream from the jet for the nonuniform conditions. The nonuniform exit conditions had the effect of preventing freestream N_2 penetration of the plume. For species produced by chemical reactions, such as NO, it was found that the species gradient across the plume shock was more pronounced than for the nonuniform exit conditions. Higher NO concentrations were observed as a result of greater relative velocities of freestream O and plume N_2.

The jet-atmosphere interaction structure showed significant changes for variations of the freestream altitude from 80 to 160 km. At 80 km the flowfield exhibits continuumlike features such as an oblique shock wave and a normal plume shock, whereas by 120 km the shock structure is much more diffuse. At the highest altitude considered here, 160 km, the plume/atmospheric interaction shock is replaced by a much diffuser interaction zone. The hydroxyl radical, a species formed by chemical reactions between plume and freestream species, was found to exist mainly in the plume/atmospheric interaction region. It was found that the OH concentration at the three altitudes was approximately proportional to freestream number density.

The change of vehicle velocity was also found to affect the flowfield structure. As the freestream velocity was increased, it was found that the shock temperature increased and the location of the shock moved closer to the body. Concentrations of chemically produced species such as NO and OH also increased at higher velocities. The importance of different chemical reactions that produce OH is difficult to assess because of to the lack of reaction cross-section and rate data at high collision energies between O and HCl.

Finally, the spatial distribution of molecular UV emission was examined, and results were presented for OH. Generally, the spatial distribution of the OH radiation was found to follow the jet/atmospheric interaction shock structure. The examination of UV emission from the jet/atmospheric interaction shock suggests that UV radiation should be detectable for onboard instruments such as were flown on the Bow Shock Ultraviolet Experiments.[26] The production of excited state species by chemiluminescent reactions has not been considered here and can be an important source, especially at the higher velocities. These processes will be considered in future work.

Acknowledgments

The research at Pennsylvania State University was supported by Space and Naval Warfare Systems Center San Diego Grant DUNS:04-399-0498 and Army Research Office Grants DAAG55-98-1-009 and DAAD19-02-1-0196. These programs are supported by the Science and Technology Directorate of the Missile Defense Agency, which is conducting programs to characterize and measure the optical radiation from rocket plumes with high spatial resolution. We specifically thank Clifton Phillips for his assistance in securing computer time on the U.S. Department of Defense High-Performance Super Computers, without which these calculations would not be possible. We are also thankful to David Campbell for helpful discussions.

References

[1]Chamberlain, R., Dang, A., and McClure, D., "Effect of Exhaust Chemistry on Reaction Jet Control," AIAA Paper 99-0806, Jan. 1999.

[2]Srivastava, B., "Lateral Jet Control of a Supersonic Missile: CFD Predictions and Comparison to Force and Moment Measurements," AIAA Paper 97-0639, Jan. 1997.

[3]Thoenes, J., "Semi-Empirical Prediction of Lateral Control Jet Flowfield Features in Hypersonic Flow," AIAA Paper 99-0805, Jan. 1999.

[4]Hudson, D., Trolier, J., and Harris, T., "Hot Jet and Mach Number Effects on Jet Interactions Upstream Separation," *AIAA Missile Sciences Conference Proceedings*, AIAA, Reston, VA, 1998, pp. 654–665.

[5]Holden, M. S., Walker, B. J., Parker, R., and Bergmann, R., "Experimental Studies of the Effects of Combustion on the Characteristics of Jet Interaction on Interceptor Performance in Supersonic and Hypersonic Flows," AIAA Paper 99-0808, Jan. 1999.

[6]Ebrahimi, H. B., "Numerical Simulation of Transient Jet-Interaction Phenomenology in a Supersonic Freestream," *Journal of Spacecraft and Rockets*, Vol. 37, No. 6, 2000, pp. 713–719.

[7]Kennedy, K., Walker, B., and Mikkelsen, C., "Jet Interaction Effects on a Missile with Aerodynamic Control Surfaces," AIAA Paper 99-0807, Jan. 1999.

[8]Roger, R. P., "The Aerodynamics of Jet Thruster Control for Supersonic/Hypersonic Endo-Interceptors: Lessons Learned," AIAA Paper 99-0807, Jan. 1999.

[9]Robinson, M. A., "Application of CFD to BMDO JI Risk Mitigation: External Burning," AIAA Paper 99-0803, Jan. 1999.

[10]Tartabini, P. V., Wilmoth, R. G., and Rault, D. F. G., "Direct Simulation Monte Carlo Calculation of a Jet Interaction Experiment," *Journal of Spacecraft and Rockets*, Vol. 32, No. 1, 1995, pp. 75–83.

[11]Glass, C. E., and LeBeau, G. J., "Numerical Study of a Continuum Sonic Jet Interacting with a Rarefied Flow," AIAA Paper 97-2536, June 1997.

[12]Glass, C. E., "A Parametric Study of Jet Interactions with Rarefied Flows," *21st International Symposium on Rarefied Gas Dynamics*, edited by R. Brun, R. Campargue, R. Gatignol, and J.-C. Lengrand, Vol. 1, Cepadues Editions, Toulouse, France, 1998, pp. 615–622.

[13]Gimelshein, S. F., Alexeenko, A. A., and Levin, D. A., "Modeling of the Interaction of a Side Jet with a Rarefied Atmosphere," *Journal of Spacecraft and Rockets*, Vol. 39, No. 2, 2002, pp. 168–176.

[14]Levin, D., Collins, R., Candler, G., Wright, M., and Erdman, P., "Examination of OH Ultraviolet Radiation from Shock-Heated Air," *Journal of Thermophysics and Heat Transfer*, Vol. 10, No. 2, 1996, pp. 200–208.

[15]Smith, T., and Ziegler, D., "Interceptor Sensor Self-Blinding Analysis of Candidate Propellants," 1999 AIAA/BMDO Technology Readiness Conf., July 1999.

[16]Moss, J. N., Bird, G. A., and Dogra, V. K., "Nonequilibrium Thermal Radiation for an Aeroassist Flight Experiment Vehicle," AIAA Paper 88-0081, Jan. 1988.

[17]Bose, D., and Candler, G. V., "Thermal Rate Constants of the $N_2 + O \rightarrow NO + N$ Reaction Using Ab Initio ^{3}A" and ^{3}A' Potential Energy Surfaces," *Journal of Chemical Physics*, Vol. 104, No. 8, 1996, pp. 2825–2833.

[18]Bird, G. A., *Molecular Gas Dynamics and the Direct Simulation of Gas Flows*, Clarendon Press, Oxford, 1994.

[19]GASP, The General Aerodynamic Simulation Program, Computational Flow Analysis Software for the Scientist and Engineer, User's Manual, Ver. 3, Aerosoft Co., Blacksburg, VA, May 1996.

[20]Ivanov, M. S., Markelov, G. N., and Gimelshein, S. F., "Statistical Simulation of Reactive Rarefied Flows: Numerical Approach and Applications," AIAA Paper 98-2669, June 1998.

[21]Bird, G. A., "Monte-Carlo Simulation in an Engineering Context," *Rarefied Gas Dynamics*, edited by S. Fisher, Vol. 74, Progress in Astronautics and Aeronautics, AIAA, New York, 1981, pp. 239–255.

[22]Borgnakke, C., and Larsen, P. S., "Statistical Collision Model for Monte Carlo Simulation of Polyatomic Gas Mixture," *Journal of Computational Physics*, Vol. 18, 1975, pp. 405–420.

[23]Gimelshein, S. F., Levin, D. A., and Collins, R. J., "Modeling of Spacecraft Glow Radiation in Flows About a Reentry Vehicle at High Altitudes," *Journal of Thermophysics and Heat Transfer*, Vol. 14, No. 4, 2000, pp. 471–479.

[24]Levin, D. A., Laux, C. O., and Kruger, C. H., "A General Model for the Spectral Calculation of OH Radiation in the Ultraviolet," *Journal of Spectroscopic Radiative Transfer*, Vol. 61, No. 3, 1999, pp. 377–392.

[25]Park, C., "Calculation of Nonequilibrium Radiation in the Flight Regimes of Aero-Assisted Orbital Transfer Vehicles," *Thermal Design of Aero-Assisted Orbital Transfer Vehicles*, edited by H. F. Nelson, Vol. 96, Progress in Astronautics and Aeronautics, AIAA, New York, 1985.

[26]Levin, D., Candler, G., Collins, R., Erdman, P., Zipf, E., and Howlett, C., "Examination of Theory for the Bow Shock Ultraviolet Rocket Experiments-I," *Journal of Thermophysics and Heat Transfer*, Vol. 8, No. 3, 1994, pp. 447–452.

[27]Mahmud, K., Kim, J., and Fontijn, A., "A High-Temperature Photochemical Kinetics Study of the Oxygen Atom + Hydrogen Chloride Reaction from 350 to 1980 K," *Journal of Physical Chemistry*, Vol. 94, No. 7, 1990, pp. 2994–2998.

[28]Hsiao, C., Lee, Y., Wang, N., Wang, J., and Lin, M., "Experimental and Theoretical Studies of the Rate Coefficients of the Reaction $O(^3P) + HCl$ at High Temperatures," *Journal of Physical Chemistry A*, Vol. 106, 2002, pp. 10,231–10,237.

[29]Bird, G. A., "Simulation of Multi-Dimensional and Chemically Reacting Flows," *Rarefied Gas Dynamics*, Vol. 1, edited by R. Campargue, Commissariat a l'Energie Atomique, Paris, 1979, pp. 365–388.

A. Ketsdever
Associate Editor